Correlations among size, defects, and photoluminescence in ZnO nanoparticles

Gang Xiong, U. Pal, and J. Garcia Serrano

Citation: Journal of Applied Physics **101**, 024317 (2007); doi: 10.1063/1.2424538
View online: http://dx.doi.org/10.1063/1.2424538
View Table of Contents: http://scitation.aip.org/content/aip/journal/jap/101/2?ver=pdfcov
Published by the AIP Publishing

Correlations among size, defects, and photoluminescence in ZnO nanoparticles

Gang Xiong[a)]
Department of Physics, Wake Forest University, Winston Salem, North Carolina 27109 and Pacific Northwest National Laboratory, Richland, Washington 99352

U. Pal[b)] and J. Garcia Serrano
Instituto de Fisica, Universidad Autonoma de Puebla, Apdo. Postal J-48, Puebla, Pue. 72570, Mexico

(Received 15 October 2006; accepted 5 November 2006; published online 22 January 2007)

We studied the correlations among size, defects, and photoluminescence emissions in ZnO nanoparticles of sizes ranging from 25 to 73 nm. The impurities and defects were characterized by Fourier-transform infrared spectroscopy and Raman spectroscopy. Particles of larger size revealed fewer surface impurities and enhanced E_2 mode of hexagonal ZnO crystals, while the oxygen vacancy centers did not vary significantly with particle size. A simultaneous increase of excitonic luminescence and defect luminescence intensities with the increase of particle size is shown, indicating both emissions are subjected to nonradiative quenching by near surface defects. The study on the size-dependent green luminescence in our samples suggests that the emission might be a bulk property instead of having a surface origin in nanostructured ZnO. Two different radiative recombination processes are involved in the excitonic emission of ZnO. While the slow decay component (370 ps) did not depend on particle size, the fast component varied from 56 to 96 ps. We attribute the slow component to free exciton recombination, while the fast component is attributed to near surface exciton recombination. © *2007 American Institute of Physics*.
[DOI: 10.1063/1.2424538]

I. INTRODUCTION

ZnO has attractive properties for possible applications in blue light emitting devices,[1] photocatalysis,[2] and dye-sensitized solar cell.[3] Understanding the roles of defects and especially surface defects are important for these applications utilizing nanostructured ZnO. The surface defects, either intrinsic or due to unintentional doping (impurities), are often found to reduce the performance for such applications. For example, surface impurities such as hydroxyl are known to quench the exciton luminescence in ZnO.[4] The surface defects can also prevent efficient charge transfer between ZnO and adsorbed molecules at the interfaces. The most obvious trend versus particle size is that the surface-to-volume ratio increases for smaller particles and the transport distance from any interior point to surface traps and recombination sites decreases in the same trend. In addition to the correlations between the defects and the optical properties, one should also notice that at nanoscale the size not only directly impacts the defect contents but also the optical properties of materials. As a matter of fact, unlike the luminescence properties of bulk crystals which have been well characterized, the photoluminescence (PL) spectra of nanostructured ZnO largely depend on synthesis methods, crystallite size and structures, and probably the most important, the defect contents in bulk and surfaces.[4–14] Examining nanoparticle ZnO PL spectra provides a way for us to understand the roles of size and defects in the earlier photoexcited processes.

In this article, we report the defects and PL in ZnO nanoparticles ranging from 25 to 73 nm. The particle sizes discussed are in the weak exciton confinement range, where exciton wave function coherence may be expected to achieve some enhancement of oscillator strength,[15] where bulk ZnO properties may begin to be approached, and yet where surface trapping, quenching, and other dead-layer effects can still be significant. Little quantum confinement effect should be expected for these samples since the sizes are much larger than the exciton Bohr radius in ZnO (approximately 2.34 nm).[10] In our investigation, the defect and impurity contents were characterized by Fourier-transfer infrared spectroscopy (FTIR) and Raman spectroscopy. It was found that in our set of samples the dominated surface defects/impurities are hydroxyl, carboxylate, and alkane. An enhancement of E_2 mode of hexagonal ZnO crystal for particles of larger size was also observed from Raman spectra. No significant variation in oxygen vacancy content was found among the samples. Time-integrated and time-resolved PL spectra were measured. We discuss the correlations among the particle sizes, the defects/impurities, and the measured PL spectra.

II. EXPERIMENT

Four ZnO nanoparticle samples of sizes ranging from 25 to 73 nm were used in this study. Provided by Nanophase Technologies Corporation, the samples were synthesized via a plasma synthesis technique.[16] The samples were labeled according to their measured specific surface area (SSA), namely BET14, BET18, BET29, and BET50, measured in the unit of m^2/g. Given the SSA numbers, the particle sizes can be calculated, as shown in the second row of Table I.

[a)]Electronic mail: xiong.g@gmail.com
[b)]Author to whom correspondence should be addressed; electronic mail: upal@sirio.ifuap.buap.mx

TABLE I. The particle sizes measured by SSA and XRD analysis.

Particle size	BET14 (nm)	BET18 (nm)	BET29 (nm)	BET50 (nm)
SSA	77	60	37	21
XRD	69	55	49	29
Average	73	58	43	25

X-ray diffraction (XRD) experiments were performed on a high-resolution, double-crystal Philips XPert MRD system. XRD revealed zincite (hexagonal) structure of ZnO nanoparticles (Fig. 1). It can be found that the full width at half maximum of the diffraction peaks decrease for the samples of larger crystallite size. The particle sizes can also be derived by XRD peak profile analysis using Scherrer's method. According to Table I, the sizes obtained by both techniques are in reasonably good agreement. The average particle sizes determined by considering the two methods are shown in the last row of Table I and will be referred to as the average particle size of the samples throughout the article.

FTIR spectra were acquired on a Perkin-Elmer Spectrum GX FTIR spectrometer. A Perkin Elmer NIR Spectrum GX FT-Raman spectrometer with a Nd-yttirium-aluminum-garnet laser source (1064 nm, 2 W) was used for recording Raman spectra of the samples. For the PL measurement, the ZnO nanoparticles were mechanically sandwiched between two *S*1 quartz slides. A sufficient amount of nanoparticles was used to ensure that the prepared samples were optically dense. Time-integrated PL spectra were excited by the third harmonic of an unamplified Ti:sapphire oscillator (273 nm, 76 MHz). The corresponding laser radiance was 6.4 W/cm^2 (peak intensity 650 kW/cm^2), and the pulse energy was approximately 8×10^{-14} J. For time-resolved PL study, a Ti:sapphire laser amplifier was used (273 nm, 250 fs, 10 Hz). The laser irradiance was approximately 3 mW/cm^2 (peak intensity $\sim$1 GW/cm^2), with pulse energy approximately of 3×10^{-10} J. The temporal and energy spectra of ZnO luminescence were captured by a streak camera (Hamamatsu C2830 temporal disperser). The temporal resolution of the streak camera was measured as $\pm$13 ps including trigger jitter.[17] All PL experiments were conducted at room temperature.

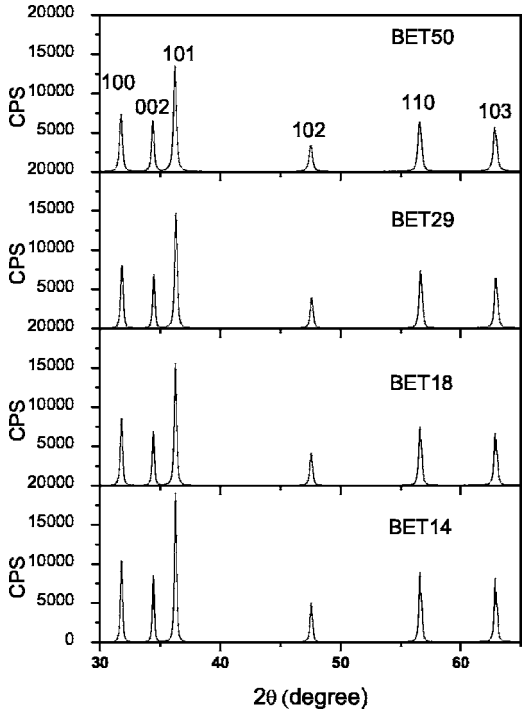

FIG. 1. The XRD graphs of ZnO nanoparticle samples.

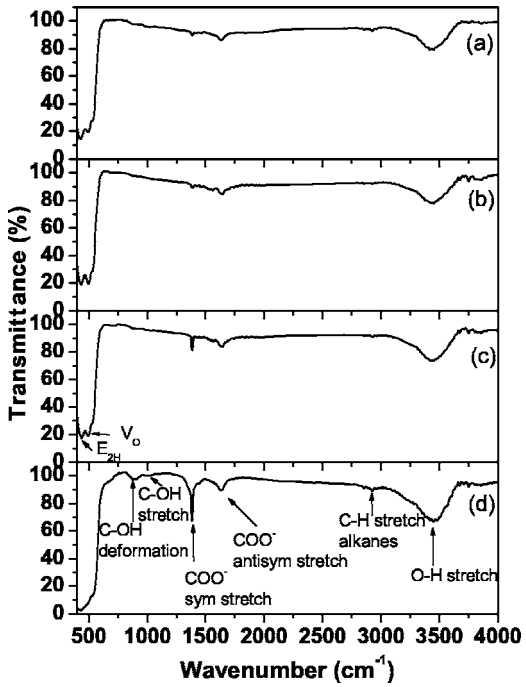

FIG. 2. FTIR spectra of the ZnO BET samples: (a) BET14, (b) BET18, (c) BET29, and (d) BET50.

III. RESULTS AND DISCUSSIONS

A. Infrared spectra

Figure 2 shows the IR spectra of the ZnO samples. A series of absorption peaks from 1000 to 4000 cm^{-1} can be found, corresponding to the vibration modes of impurities such as hydroxyl, carboxylate, and alkane in the materials. To be more specific, a broadband at 3500 cm^{-1} is assigned to the OH stretching mode of hydroxyl group. Peaks between 2830 and 3000 cm^{-1} are due to C-H stretching vibration of alkane groups. The peaks observed at 1630 and 1384 cm^{-1} are due to the asymmetrical and symmetrical stretching of the zinc carboxylate (COO-), respectively. At least two absorption bands due to C-OH bond are observed at 1095 and 890 cm^{-1} correspond to stretching and deformation modes, respectively, especially for the BET50 sample. As the size of the nanoparticles increases, the FTIR signatures of these impurities decrease. The carboxylate probably comes from reactive carbon-containing plasma species during synthesis and the hydroxyl results from the hygroscopic nature of ZnO.[18] Together these suggest that the FTIR-identified impurities mainly exist near particle surfaces.

For all the samples under study, two strong absorption bands are observed at 437 and 505 cm^{-1}. While the band at 437 cm^{-1} corresponds to the E_2 mode of hexagonal ZnO (Raman active), the band at 505 cm^{-1} is associated with oxy-

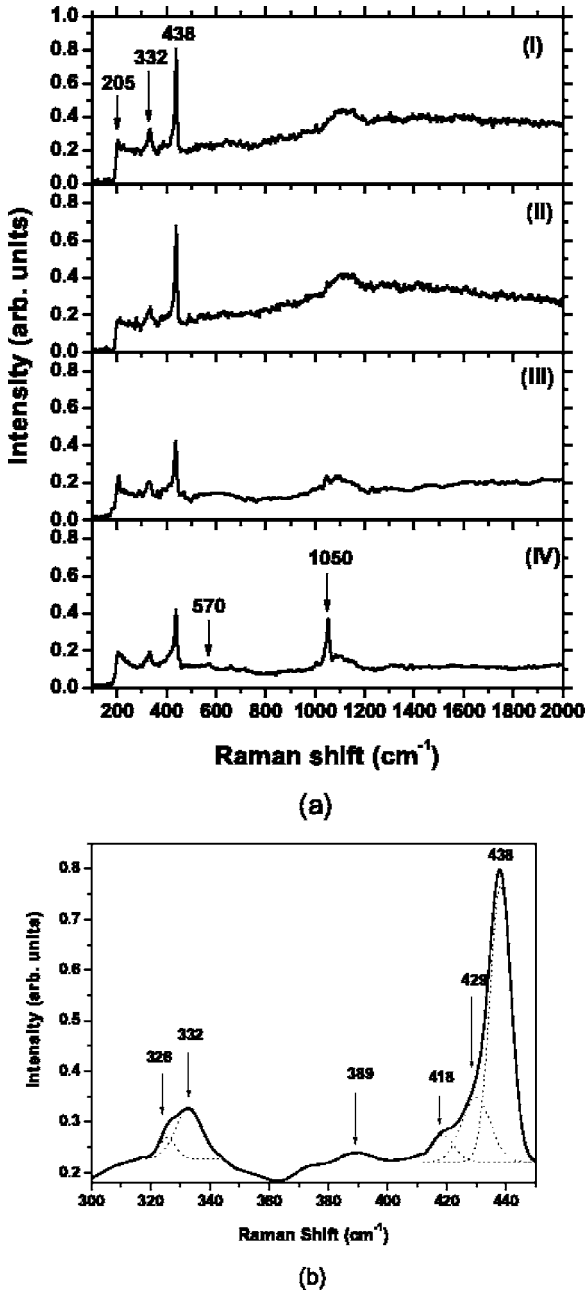

FIG. 3. (a). Raman spectra of the ZnO BET samples: (I) BET14, (II) BET18, (III) BET29, and (IV) BET 50. (b) Peak assignments for the BET14 sample in the range from 300 to 450 cm^{-1}.

gen vacancy defect complex in ZnO.[19] The intensity of the oxygen-vacancy related defect-complex band does not appear to change much versus particle size, indicating they are probably bulk defects.

B. Raman spectra

Figure 3 shows the Raman spectra of the ZnO BET samples. The spectra exhibit three asymmetrical bands at 205, 332, and 438 cm^{-1}. The bands at 205 and 332 cm^{-1} are due to multiphonon processes and have been assigned to the $2\text{-}TA(M)$ and $2\text{-}E_2(M)$ modes, respectively.[20] The peak at 438 cm^{-1} corresponds to the E_2 mode, typical to the hexagonal phase of ZnO.[21,22] A remarkable increase in the E_2 mode intensity is observed for samples of larger particle sizes. A very weak peak at 570 cm^{-1} is associated with oxygen deficiency in the ZnO lattices. The spectrum of the BET50 sample also revealed a sharp peak at 1050 cm^{-1}, attributed to the C-O asymmetric stretching mode of carboxylate group. The intensity of the 1050 cm^{-1} peak decreases notably in the BET29 spectrum and nearly disappears from the BET18 and BET14 spectra. This is also evident from IR analysis. In short summary, an enhanced E_2 mode originated from the hexagonal ZnO is found for samples of large particle sizes. In addition, the C-O asymmetric stretching-mode (1050 cm^{-1}) of the carboxylate defect mode decreases. The Raman results indicate better crystallinity, lower carboxylate and hydroxyl impurity contents in the samples of larger particle sizes.

TABLE II. The assignments of the observed Raman peaks for ZnO nanoparticle samples.

Peak (cm^{-1}) Present work	Peak (cm^{-1}) Literature	Assignment
205	208,[a] 209[b]	$2\text{-}TA(M)$
326	321[c]	$3E_{2L}$
332	332,[a] 331[b]	$2\text{-}E2(M)$, $E_{2H}\text{-}E_{2L}$
389	380,[d] 392[b]	A_{1T}
418	413,[d] 410[e]	$E_1(TO)$
429	426[c]	E_{1T}
438	439,[e] 437[c]	E_{2H}

[a]See Ref. 20.
[b]See Ref. 25.
[c]See Ref. 22.
[d]See Ref. 26.
[e]See Ref. 27.

From the Gaussian fittings of the asymmetric bands, several Raman peaks are extracted and listed in Table II. The discrepancies between the observed phonon frequencies with the corresponding reported ones for bulk ZnO, especially for the $E_1(TO)$ mode are probably due to nanocrystalline nature of our samples. As has been demonstrated by Fonoberov and Balandin,[23,24] the confined optical phonons in wurtzite nanocrystals have a discrete spectrum of frequencies, different from those in bulk crystals.

C. PL excited by unamplified Ti:sapphire (8×10^{-14} J per pulse)

Figure 4(a) shows the PL spectra of the samples with an excitation energy of 8×10^{-14} J per pulse. Each spectrum consists of a broad peak at the visible region. For the 73-nm sample (BET14), the visible peak is centered at 2.5 eV, generally known as the green defect luminescence in ZnO. As the particle size becomes smaller, this peak becomes flatter over the entire visible region and gradually shifts to higher energy. This energy shift is likely due to the appearance of a 2.8-eV peak for particles of smaller size, of which the origin is still to be understood.[28,29] The peak located at approximately 3.26 eV is attributed to the phonon replicas of exciton luminescence.[30]

We plot the integrated intensities of both the exciton and defect luminescence band in Fig. 4(b). The intensities of both PL bands increase monotonically upon the increase of particle size. It appears that although the luminescent mecha-

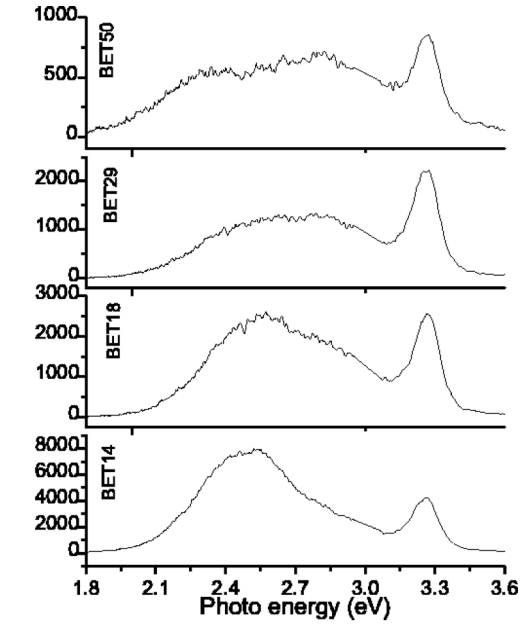

FIG. 4. (a) The photoluminescence spectra of ZnO nanoparticles excited by 273 nm Ti:sapphire laser (pulse energy 8×10^{-14} J). The exciton PL peak is centered at 3.26 eV, while the defect luminescence peak shifts toward to blue as the particle size gets smaller. (b) The PL intensity versus particle size plots.

nisms for these two bands are very different, their quantum yields are partially limited by some nonradiative processes. This is in good agreement with the measured FTIR and Raman spectra, which showed that larger ZnO nanoparticles have better crystalline quality and less surface impurities. These lattice defects and surface impurities (such as hydroxyl, carboxylate, and alkane) likely serve as nonradiative recombination or trapping centers to compete with radiative recombination. For example, surface hydroxyl groups usually act as hole scavengers to quench the PL in ZnO (Ref. 4) as well as in other metal-oxide semiconductors.[31]

Presently, the most recognized hypothesis on the origin of the green luminescence in ZnO involves the radiative recombination of electrons captured at oxygen vacancy sites with trapped holes.[32] In our study, both the exciton and defect PL intensity increases versus the particle size. This observation is exactly opposite to some other experiments reported in the literature.[11,12] For example Dijken *et al.* reported a decrease of the green luminescence intensity upon increasing the size of ZnO quantum dots, while the exciton luminescence increases. They suggested that the holes contributed to the green luminescence are primarily trapped at the surface.[12] Similar observation was also reported by Shalish *et al.*, who proposed a surface recombination mechanism for the green luminescence of ZnO.[11] However, the sizes of our samples are approximately two orders of magnitude larger than the samples investigated by Dijken (0.7–1 nm).[12] Thus trapped electron tunneling to the surface can be a significant source contributing to the green luminescence in quantum dots, as observed by Dijken,[12] but probably not for particles of much larger size in our study (25–73 nm) and others (50–300 nm).[11] It is because that the probability of tunneling recombination between a surface trapped hole and an ionized oxygen vacancy center decreases rapidly versus the distance, due to the limited wave function overlapping between trapped electrons and holes. Furthermore, there exist less surface states per volume for a larger particle, which also discourages surface recombination. Therefore, we believe that the majority of carriers (including localized holes) responsible for the green luminescence in our samples are trapped within the nanocrystallites, similar to the green luminescence observed in bulk crystal. This agrees with the FTIR and Raman studies, which showed no significant fluctuation in oxygen vacancy concentration among our samples, while the defect quenching centers mainly exist near surfaces and are strongly size dependent. In conclusion, in our samples, surface quenching plays a dominated role in determination of the defect luminescence intensity. This is in agreement with a recent report by Fonoberov *et al.* who also found a similar trend in the visible luminescence band of ZnO quantum dots (4 nm), nanocrystals (20 nm), and bulk crystal.[33] The difference between our results and Ref. 11 (samples of 50–300 nm in size) may be attributed to the sample differences in exterior and surface defect/impurity content.

D. PL excited by amplified Ti:sapphire (3×10^{-10} J per pulse)

The time-integrated photoluminescence spectra of ZnO nanoparticles excited by the 273-nm amplified Ti:sapphire laser are plotted in Fig. 5(a). Unlike the spectra excited by the unamplified Ti:sapphire laser, we found that the visible defect luminescence is practically absent in the spectra excited by the amplified Ti:sapphire. Therefore, in the spectra of Fig. 5 only the excitonic luminescence is shown. The pulse energy of the amplified Ti:sapphire is approximately 4000 times stronger than the unamplified Ti:sapphire. Guo *et al.* showed that the green emission saturates with excitation intensity because of dilute defect involvement.[34] Due to saturation of the green defect luminescence, the photoluminescence spectra excited by the amplified Ti:sapphire are dominated by the ultraviolet band edge luminescence. The excitation intensity is still below the lasing threshold, so the "exciton" PL characteristics remain, similar to the spectra excited by the unamplified laser. Once again the peak inten-

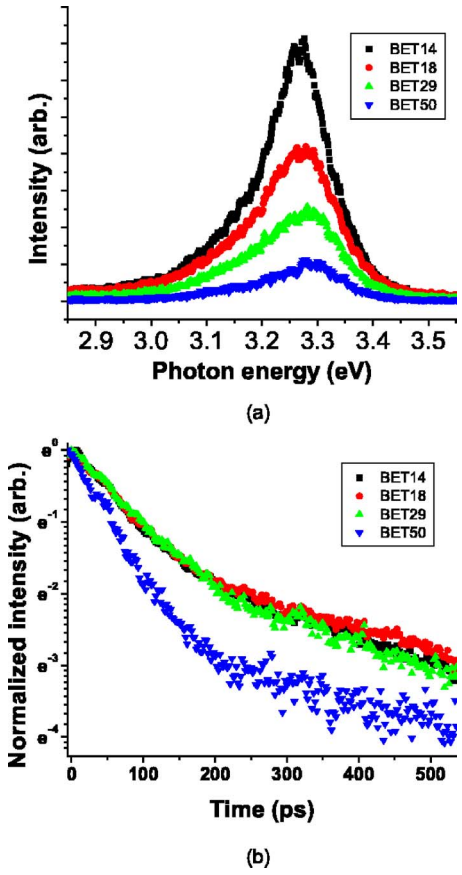

FIG. 5. (Color online) (a) The photoluminescence spectra of ZnO nanoparticle samples excited by 273 nm Ti:sapphire laser (pulse energy 3×10^{-10} J). The green luminescence was absent under this excitation. Therefore, only the excitonic luminescence (3.26 eV) is shown in this figure. (b) The double-exponential photoluminescence decay of ZnO nanoparticles. The intensities are normalized and plotted in logarithmic scale.

sity versus particle size relationship is reproduced in agreement with the observed PL excited at lower intensity.

We plot the decay spectra of normalized luminescence intensities in Fig. 5(b). For spectrum of each sample, the decay profile can be fitted into a double exponential function. From Fig. 5(b) we can see the fast components (τ_1) of BET14, BET18, and BET29 are very similar to each other. The fittings gave the exponential decay time of around 96 ps for all the three samples of bigger particle size. However, the fast component of BET50, is significantly smaller, around 56 ps. The slow components (τ_2) are around 370 ps for all four samples. Apparently two different recombination processes are involved in the excitonic emission of ZnO at room temperature. The double-exponential decay of exciton luminescence in ZnO has been previously reported with similar lifetime values.[6,7,35–37] However, the exact exciton decay mechanisms are still under some debate.[35,36]

The slow decay component is be independent from the particle size and defect/impurity content in ZnO. The results suggest that the slow component is due to the free exciton recombination that occurred inside the bulk of the nanoparticles. We have previously measured the free exciton luminescence lifetime in ZnO single crystal to be 400 ps,[38] compared to 370 ps in these nanoparticle samples. This assignment is also in agreement with the report by Guo *et al.*[37] The subpicosecond exciton lifetime in ZnO is benefited from the enhancement of oscillator strength (exciton coherence). The exciton coherent volume in our samples is possibly determined by exciton scattering length mediated by bulk defects, thus we did not see any size dependence in terms of free exciton lifetime.

We attribute the fast component to the radiative recombination of near surface exciton. Due to the presence of surface defects/impurities, the surface exciton recombination is subject to nonradiative quenching, thus a faster decay time is expected. A revisit to the FTIR spectra show that the BET50 sample (smallest) has far larger defect/impurity content than any other samples. As the result, the faster component of BET50 is the smallest. The qualitative defect/impurity content in other samples varies but are more or less comparable. This size dependence is reflected by the PL intensity versus size plot. However, within the temporal resolution of our streak camera (13 ps), the variation of slow component (96 ps) is practically indistinguishable.

IV. SUMMARY

We have investigated the PL and the defects/impurities in ZnO nanoparticles of sizes varied from 25 to 73 nm. FTIR and Raman spectra showed that the primary near surface defects in our ZnO nanoparticle samples are hydroxyl, carboxylate, and alkane. Oxygen vacancy content appeared to be size independent and is considered as bulk defects. Raman spectroscopy also indicated better crystalline quality for samples of large particle size. The intensities of the excitonic and defect luminescence simultaneously increase with the increase of particle size, indicating a similar mechanism is responsible for quenching both emissions. From the correlation between the PL and the defects revealed by FTIR and Raman spectra, it seems that the residual hydroxyl, carboxylate, and alkane groups act as nonradiative recombination centers in ZnO nanoparticles. The size dependence of green luminescence intensity suggests that the green luminescence is more likely a bulk property associated with oxygen vacancy in our nanoparticle ZnO rather than having a surface origin.

Time-resolved PL study on the exciton luminescence showed a double-exponential decay profile. While the fast component varies from 56 to 96 ps, the slow component remains nearly the same (370 ps) for all the samples. We attribute the fast component to the recombination of surface exciton partially quenched by near surface defects/impurities. The slow component is due to the radiative recombination of free excitons.

ACKNOWLEDGMENTS

The authors would like to thank Nanophase Corporation for providing them with the ZnO samples for study. U.P. thanks CONACyT, Mexico for its partial financial help through Grant No. 46269. They thank Dr. R. T. Williams for discussion.

[1]S. J. Jiao *et al.*, Appl. Phys. Lett. **88**, 031911 (2006).
[2]E. Pelizzetti, C. Minero, P. Piccinini, and M. Vincenti, Coord. Chem. Rev. **125**, 183 (1993).

[3]K. Kakiuchi, E. Hosono, and S. Fuiihara, J. Photochem. Photobiol., A **179**, 81 (2006).
[4]H. Zhou, H. Alves, D. M. Hofmann, W. Kriegseis, B. K. Meyer, G. Kaczmarczyk, and A. Hoffmann, Appl. Phys. Lett. **80**, 210 (2002).
[5]G. Xiong, J. Wilkinson, J. Lyles, K. B. Ucer, and R. T. Williams, Radiat. Eff. Defects Solids **158**, 83 (2003).
[6]H. Priller *et al.*, J. Lumin. **112**, 173 (2005).
[7]S. Hong, T. Joo, W. I. Park, Y. H. Jun, and G.-C. Yi, Appl. Phys. Lett. **83**, 4157 (2003).
[8]T. Hirai, Y. Harada, S. Hashimoto, T. Itoh, and N. Ohno, J. Lumin. **112**, 196 (2005).
[9]D. Millers, L. Grigorjeva, W. Lojkowski, and T. Strachowski, Radiat. Meas. **38**, 589 (2004).
[10]Y. Gu, I. Kuskovsky, M. Yin, S. O'Brien, and G. F. Neumark, Appl. Phys. Lett. **85**, 3833 (2004).
[11]I. Shalish, H. Temkin, and V. Narayanamurti, Phys. Rev. B **69**, 245401 (2004).
[12]A. van Dijken, J. Makkinje, and A. Meijerink, J. Lumin. **92**, 323 (2001).
[13]P. Zu, Z. K. Tang, G. K. L. Wong, M. Kawasaki, A. Ohtomo, H. Koinuma, and Y. Segawa, Solid State Commun. **103**, 459 (1997).
[14]U. Pal, J. Garcia-Serrano, P. Santiago, G. Xiong, K. B. Ucer, and R. T. Williams, Opt. Mater. (Amsterdam, Neth.) **29**, 65 (2006).
[15]G. Xiong, J. Wilkinson, K. B. Ucer, and R. T. Williams, J. Lumin. **112**, 1 (2005).
[16]Nanophase Technologies Corporation, 1319 Marquette Drive, Romeoville, IL 60446.
[17]G. Xiong, J. Wilkinson, K. B. Ucer, and R. T. Williams, J. Phys.: Condens. Matter **17**, 7287 (2005).
[18]R. Brotzman (private communication).
[19]A. Kaschner *et al.*, Appl. Phys. Lett. **80**, 1909 (2002).
[20]J. M. Calleja and M. Cardona, Phys. Rev. B **16**, 3753 (1977).
[21]G. J. Exarhos and S. V. Sharma, Thin Solid Films **270**, 27 (1995).
[22]Y. J. Xing, Appl. Phys. Lett. **83**, 1689 (2003).
[23]V. A. Fonoberov and A. A. Balandin, Phys. Rev. B **70**, 233205 (2004).
[24]V. A. Fonoberov and A. A. Balandin, J. Phys.: Condens. Matter **17**, 1085 (2005).
[25]M. Rajalakshmi, A. K. Arora, B. S. Bendre, and S. Mahamuri, J. Appl. Phys. **87**, 2445 (2000).
[26]C. Arguello, D. Rousseau, and S. Porto, Phys. Rev. **181**, 1351 (1969).
[27]K. Alim, V. Fonoberov, and A. Balandin, Appl. Phys. Lett. **86**, 053103 (2005).
[28]Y. W. Heo, M. Kaufman, K. Pruessner, D. P. Norton, F. Ren, M. F. Chisholm, and P. H. Fleming, Solid-State Electron. **47**, 2269 (2003).
[29]D. H. Liu, L. Liao, J. C. Li, H. X. Guo, and Q. Fu, Mater. Sci. Eng., B **121**, 77 (2005).
[30]The free *A* exciton recombination is strongly absorbed thus it does not show up in the spectrum.
[31]Z. Zhang, C. Boxall, and G. Kelsall, Colloids Surf., A **73**, 145 (1993).
[32]K. Vanheusden, W. L. Warren, C. H. Seager, D. R. Tallant, and J. A. Voigt, J. Appl. Phys. **79**, 7983 (1996).
[33]V. A. Fonoberov, K. A. Alim, and A. A. Balandin, Phys. Rev. B **73**, 165317 (2006).
[34]C. Guo, Z. Fu, and C. Shi, Chin. Phys. Lett. **16**, 146 (1999).
[35]S. W. Jung, W. I. Park, H. D. Cheong, G.-C. Yi, and H. M. Jang, Appl. Phys. Lett. **80**, 1924 (2002).
[36]W. M. Kwok, A. B. Djurisic, Y. H. Leung, W. K. Chan, and D. L. Phillips, Appl. Phys. Lett. **87**, 223111 (2005).
[37]B. Guo, Z. Ye, and K. S. Wong, J. Cryst. Growth **253**, 252 (2003).
[38]J. Wilkinson, K. B. Ucer, and R. T. Williams, Radiat. Meas. **38**, 501 (2004).